Article

Bond or Cage Effect: How Nitrophorins Transport and Release Nitric Oxide

Marcelo A. Mart, Mariano C. Gonzlez Lebrero, Adrin E. Roitberg, and Dario A. Estrin

J. Am. Chem. Soc., **2008**, 130 (5), 1611-1618 • DOI: 10.1021/ja075565a

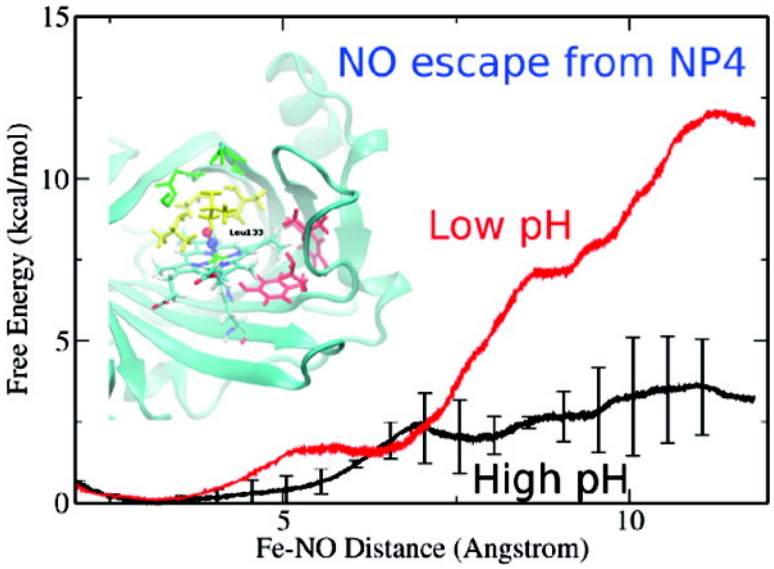

More About This Article

Additional resources and features associated with this article are available within the HTML version:

- Supporting Information
- Links to the 1 articles that cite this article, as of the time of this article download
- Access to high resolution figures
- Links to articles and content related to this article
- Copyright permission to reproduce figures and/or text from this article

View the Full Text HTML

J|A|C|S
ARTICLES
Published on Web 01/12/2008

Bond or Cage Effect: How Nitrophorins Transport and Release Nitric Oxide

Marcelo A. Martí,*,† Mariano C. González Lebrero,† Adrián E. Roitberg,‡ and Dario A. Estrin†

Departamento de Química Inorgánica, Analítica, y Química Fisica, Facultad de Ciencias Exactas y Naturales, Universidad de Buenos Aires, INQUIMAE-CONICET, Ciudad Universitaria, Pab. 2, C1428EHA, Buenos Aires, Argentina, and Quantum Theory and Project and Department of Chemistry, University of Florida, Gainesville, Florida 32611-8435

Received July 25, 2007; E-mail: marcelo@qi.fcen.uba.ar

Abstract: Most blood-sucking insects possess salivary proteins which, upon injection into the victim's tissue, help them improve their feeding. One group of these salivary proteins takes advantage of the vasodilator properties of NO to perform this task. These proteins are the so-called nitrophorins (NPs). NPs are heme proteins that store and transport NO, which, when released in the victim's tissue, produces vasodilation and inhibition of blood coagulation. It has been proposed that NO binds tightly to NP at a low pH of around 5.6 and that once NPs are injected in the victims tissue, at a pH of approximately 7.4, a conformational change occurs which lowers NO affinity, allowing it to be released. In this work we have studied the NO release mechanism of NP4 at a molecular level using state of the art computer simulation techniques. We have used molecular dynamics (MD) simulations to study NP4 conformational dynamics at both pH values 5.6 and 7.4 and computed the corresponding free energy profile for NO release using a multiple steering molecular dynamics scheme. We also have used hybrid quantum mechanical/molecular mechanics (QM/MM) techniques to analyze the heme-NO structure and the Fe−NO bond strength in the different NP4 conformations. Our results provide the molecular basis to explain that NO escape from NP4 is determined by differential NO migration rates and not by a difference in the Fe−NO bond strength. In contrast to most heme proteins that control ligand affinity by modulating the bond strength to the iron, NP4 has evolved a cage mechanism that traps the NO at low pH and releases it upon cage opening when the pH rises.

Introduction

Nitric oxide (NO), a small reactive molecule, is responsible for diverse physiological functions in mammals, such as blood pressure regulation, neurotransmission, and immune response among others.[1,2] It is usually assumed that it is produced by the heme protein NO synthase (NOS),[3,4] and its main physiological receptor is another heme protein, the soluble guanylate cyclase (sGC).[5] Interestingly NO is a highly reactive molecule, capable of producing high reactive nitrogen oxide species, heme oxidation/reduction,[6,7] and tyrosine[8] and cysteine nitrations.[9] It is still debated how the NO physiological functions are accomplished avoiding toxicity due to its high reactivity.

Most blood-sucking insects possess salivary proteins which, upon injection into the victim's tissue, help them improve their feeding.[10] One group of these salivary proteins takes advantage of the vasodilator properties of NO to perform this task. These proteins are the so-called nitrophorins (NPs).[10] NPs are heme proteins that store and transport NO, which when released in the victim's tissue produces vasodilation and inhibition of blood coagulation.[11,12] One of the most studied NPs are those obtained from the salivary glands of the kissing bug *Rhodnius prolixus.* This small insect, found mostly in South America but also in North America, is a vector for the parasite *Trypanosoma cruzi*, the causative agent of Chagas Disease or American Trypanosomiasis. *R. prolixus* has the ability of transmitting *T. cruzi* to humans. It is estimated that 16 million people are infected.[13−15]

† Universidad de Buenos Aires.
‡ University of Florida.

(1) Palmer, R. M. J.; Ferrige, A. G.; Moncada, S. *Nature* **1987**, *327* (6122), 524−526.
(2) Moncada, S.; Palmer, R. M. J.; Higgs, E. A. *Pharm. Rev.* **1991**, *43* (2), 109−142.
(3) Marletta, M. A. *J. Biol. Chem.* **1993**, *268* (17), 12231−12234.
(4) Alderton, W. K.; Cooper, C. E.; Knowles, R. G. *Biochem. J.* **2001**, *357* (3), 593−615.
(5) Denninger, J. W.; Marletta, M. A. *Biochim. Biophys. Acta* **1999**, *1411* (2−3), 334−350.
(6) Laverman, L. E.; Ford, P. C. *J. Am. Chem. Soc.* **2001**, *123* (47), 11614−11622.
(7) Ford, P. C.; Fernandez, B. O.; Lim, M. D. *Chem. Rev.* **2005**, *105* (6), 2439−2455.
(8) Radi, R. *Proc. Natl. Acad. Sci. U.S.A.* **2004**, *101* (12), 4003−4008.
(9) Forman, H. J.; Torres, M.; Fukuto, J. *Mol. Cell. Biochem.* **2002**, *234−235*, 49−62.
(10) Montfort, W. R.; Weichsel, A.; Andersen, J. F. *Biochim. Biophys. Acta* **2000**, *1482* (1−2), 110−118.
(11) Ribeiro, J. M. C.; Hazzard, J. M. H.; Nussenzveig, R. H.; Champagne, D. E.; Walker, F. A. *Science* **1993**, *260* (5107), 539−541.
(12) Ascenzi, P.; Nardini, M.; Bolognesi, M.; Montfort, W. R. *Bioch. Mol. Bol. Educ.* **2002**, *30* (1), 68−71.
(13) Rassi, A., Jr.; Rassi, A.; Little, W. C. *Clin. Card.* **2000**, *23* (12), 883−9.
(14) Kirchhoff, L. V. *New. Eng. J. Med.* **1993**, *329* (9), 639−44.
(15) Beard, C. B.; Pye, G.; Steurer, F. J.; Rodriguez, R.; Campman, R.; Peterson, A. T.; Ramsey, J.; Wirtz, R. A.; Robinson, L. E. *Emerg. Inf. Dis.* **2003**, *9* (1), 103−5.

10.1021/ja075565a CCC: $40.75

Four *Rhodnius prolixus* NPs (NP1−4) have been cloned[16] and characterized spectroscopic and kinetically,[11,17] and three of them also structurally,[18−21] the most intensively studied being NP4. The results showed that all four NPs function by binding NO in a pH sensitive manner. The NO is synthesized in the salivary glands by a typical NOS[22] where it binds tightly to NP at a low pH of around 5. Once NPs are injected in the victims tissue, with a pH of approximately 7.4, a conformational change occurs which allows NO to be released.[10,17] The X-ray structural data showed that all 4 NPs have a conserved structure consisting of an eight-stranded antiparallel β-barrel typical of the lipocalin family.[23] The heme group is tightly buried in the barrel, contacting invariant residues Tyr140, Leu57, Phe68, Tyr105, Leu123, Leu133, and invariant heme proximal ligand His59.[18,19,21,24] The heme side end of the barrel is capped by the four loops AB, CD, EF, and GH. High-resolution structures of NP4 in different pH conditions reveal that the large pH induced conformational change involves mainly loops AB and GH, which open at a high pH value and thus change NO affinity.[24,25]

An important feature in the high-resolution structures of NPs was that in all of them the heme displayed significant distortions from planarity, specially ruffling and saddling deformations.[18,24,26,27] It is well-known that NO is able to interact with both ferrous (Fe^{II}) and ferric (Fe^{III}) heme proteins,[6,28] forming the corresponding $[FeNO]^7$ or $[FeNO]^6$ nitrosyl complexes in the Enemark and Feltham notation.[29] Although NO association rates are similar for both iron oxidation states, dissociation rates (k_{off}) are completely different. Fe^{II} dissociation rate constants are around 10^{-4} s^{-1} leading to very high equilibrium constants, $K_{eq} \approx 10^{11}$ M^{-1}.[6,30] On the other hand, Fe^{III} dissociation rates are larger and span a wide range from 0.1 to 40 s^{-1}, giving rise to lower equilibrium values ($K_{eq} = 10^3-10^5$ M^{-1})[6,30] Furthermore, excess NO is able to reduce Fe^{III} heme centers yielding the stable $[FeNO]^7$ complexes in a process known as reductive nitrosylation. As expected for a NO transport protein, NPs bind and release NO in the Fe^{III} state and are stable toward reductive nitrosylations when compared to Mb. This is consistent with the reduction potentials of NPs that are about 300 mV more negative than that of Mb.[17,30] The highly ruffled conformation of the heme group in NPs is supposed to be connected to the stabilization of the ferric state.[30]

Scheme 1.

$$\mathrm{NP + NO} \underset{k_{-1}}{\overset{k_1}{\rightleftharpoons}} \mathrm{NP\text{-}NO} \underset{k_{off}/k_{off2}}{\overset{k_2}{\rightleftharpoons}} \begin{matrix}\mathrm{NP'\text{-}NO}\\ \mathrm{NP''\text{-}NO}\end{matrix}$$
pH dep.

Based on the kinetics of NO binding and release for all four NPs a three-state model was proposed (Scheme 1). In this scheme, the binding and release process involves two steps. One step, characterized by kinetic constants k_1 and k_{-1}, is thought to correspond to Fe−NO binding and Fe−NO thermal bond breaking, respectively. This step is pH independent. The other step, characterized mainly by the kinetic constants k_{off} and k_{off2}, correspond to the fast and slow pH dependent observed release rate constants. NP′-NO and NP″-NO represent the species that give rise to both k_{off} values.

This analysis yielded a 7−11-fold increase in the NO dissociation equilibrium constant K_d as the pH increased from ~5 to ~7.4 due to an increase in the k_{off} values. Since no pH dependence on k_{-1} was observed, it was proposed the Fe−NO bond breaking is not involved in pH regulation and that ligand escape must be regulated through ligand migration. The origin of both phases and the nature of both NP′ and NP″ are not clear.[17] Structural support for the above scheme came from the high-resolution studies of NP4 showing the open state of AB and GH loops at higher pH.[24] Furthermore, mutant structural and kinetic studies on Asp30 corroborated the connection between AB, GH loop movement and NO escape and its pH dependence.[25] Interestingly, Asp30 mutants retained multiphase kinetics leading to the suggestion of the existence of multiple forms with different Fe−NO bond strengths.[25] Although much has been learned on the NO transport mechanism in NP, a detailed understanding of the molecular basis of the pH dependent NO release is still missing. Recently, Kondrashov et al.[31] reported a Molecular Dynamics study of NO unbound NP4 at low and high pH and compared it with myoglobin simulations. The authors found that NO was unable to escape the protein in the low pH simulations, while it escaped in two out of the six simulations performed at high pH. Even if these simulations provide valuable information regarding NP4 function, the results are qualitative and no answer is provided with respect to the discrimination of Fe−NO bonding and ligand migration effects.

The proposal that NP's NO release relies mainly on the NO escape rate makes NPs a very peculiar case among typical heme proteins. In the process of ligand release from heme proteins, as in this case, the process may be decomposed in two steps. First the iron-−igand bond (Fe−NO bond) must be broken. Second, the ligand must diffuse from the protein active site into the bulk solvent. The breadth of behaviors found in heme proteins points to a complex interplay between bond breaking and diffusion and does not show any universal behavior. In most heme proteins, the observed ligand release or dissociation rate is determined mainly by the strength by which the protein binds to the ligand, with minor contributions due to ligand migration process. This is evidenced by most NO and CO dissociation rates from ferrous heme proteins displaying similar values to

(16) Champagne, D. E.; Nussenzveig, R. H.; Ribeiro, J. M. C. *J. Biol. Chem.* **1995**, *270* (15), 8691−8695.
(17) Andersen, J. F.; Ding, X. D.; Balfour, C.; Shokhireva, T. K.; Champagne, D. E.; Walker, F. A.; Montfort, W. R. *Biochemistry* **2000**, *39* (33), 10118−10131.
(18) Andersen, J. F.; Montfort, W. R. *J. Biol. Chem.* **2000**, *275* (39), 30496−30503.
(19) Andersen, J. F.; Weichsel, A.; Balfour, C. A.; Champagne, D. E.; Montfort, W. R. *Structure* **1998**, *6* (10), 1315−1327.
(20) Weichsel, A.; Andersen, J. F.; Champagne, D. E.; Walker, F. A.; Montfort, W. R. *Nat. Struct. Biol.* **1998**, *5* (4), 304−309.
(21) Andersen, J. F.; Champagne, D. E.; Weichsel, A.; Ribeiro, J. M. C.; Balfour, C. A.; Dress, V.; Montfort, W. R. *Biochemistry* **1997**, *36* (15), 4423−4428.
(22) Ribeiro, J. M. C.; Nussenzveig, R. H. *FEBS Lett.* **1993**, *330* (2), 165−168.
(23) Flower, D. R.; North, A. C. T.; Sansom, C. E. *Biochim. Biophys. Acta* **2000**, *1482* (1−2), 9−24.
(24) Kondrashov, D. A.; Roberts, S. A.; Weichsel, A.; Montfort, W. R. *Biochemistry* **2004**, *43* (43), 13637−13647.
(25) Maes, E. M.; Weichsel, A.; Andersen, J. F.; Shepley, D.; Montfort, W. R. *Biochemistry* **2004**, *43* (21), 6679−6690.
(26) Shokhireva, T. K.; Weichsel, A.; Smith, K. M.; Berry, R. E.; Shokhirev, N. V.; Balfour, C. A.; Zhang, H.; Montfort, W. R.; Walker, F. A. *Inorg. Chem.* **2007**, *46* (6), 2041−2056.
(27) Maes, E. M.; Roberts, S. A.; Weichsel, A.; Montfort, W. R. *Biochemistry* **2005**, *44* (38), 12690−12699.
(28) Sharma, V. S.; Traylor, T. G.; Gardiner, R.; Mizukami, H. *Biochemistry* **1987**, *26* (13), 3837−43.
(29) Enemark, J. H.; Feltham, R. D. *Coord. Chem. Rev.* **1974**, *13*, 339−406.
(30) Walker, F. A. *J. Inorg. Biochem.* **2005**, *99* (1), 216−36.
(31) Kondrashov, D. A.; Montfort, W. R. *J. Phys. Chem. B* **2007**.

those observed for isolated porphyrins in aqueous solution.[6] Moreover, when O_2 is the ligand, the dissociation rate is almost entirely regulated by the Fe−O_2 and H-bond interactions with neighboring aminoacids. Contributions to the overall ligand release rate due to ligand migration processes are observed when the protein displays secondary docking sites, the so-called xenon pockets as in myoglobin.[32,33] In this context, understanding the molecular basis of the NO release mechanism in NP is of primary concern.

To shed light on this issue we have studied the NO release mechanism of NP4 at a molecular level using state-of-the-art computer simulation techniques. We have used molecular dynamics (MD) simulations to study NP4 conformational dynamics at pH values 5.6 and 7.4 and computed the corresponding free energy profile for NO release using advanced sampling techniques in both cases. All together the MD simulations amount to about a 0.15 μs simulation time. We also used hybrid quantum mechanical/molecular mechanics (QM/MM) techniques to analyze the heme-NO structure and the Fe−NO bond strength in the different NP4 conformations. Our results confirm that NP function is modulated by the differences in ligand migration and escape at different pH values and allow a molecular interpretation of this NO release mechanism.

Materials and Methods

System Setup and Equilibration. The initial structure for the MD simulations was built starting from the crystal structures of NO bound NP4 (pH = 5.6) pdb code 1X8O and NH_3 bound NP4 (pH=7.4) pdb code 1X8P.[19,24,25,27] These structures present the closed low pH and open high pH conformation of AB and GH loops respectively. Special attention was paid to the protonation state of the titratable residues since they are a key issue in modulating AB and GH loop conformation. The protonation state was assigned as suggested from previous experimental[24] and theoretical[34] works. The only residue that changed protonation state was Asp30, which was protonated at low pH and charged at high pH. As will be shown below, with this assumption, the AB and GH loops in the simulated protein retain the experimentally observed conformations.

To set up the systems for the MD simulations, the above-mentioned structures were immersed in a pre-equilibrated octahedral box of TIP3P water molecules. All simulations were performed at 1 atm and 300 K and maintained with the Berendsen barostat and thermostat,[35,36] using periodic boundary conditions and Ewald sums (grid spacing of 1 Å) for treating long-range electrostatic interactions. The SHAKE algorithm was used to keep bonds involving H atoms at their equilibrium length.[37] A 2 fs time step was used for the integration of Newton's equations. The Amber ff99SB[38] force field parameters were used for all residues, except the heme. The heme parameters used in this work were developed and thoroughly tested by our group in previous works.[33,39] All simulations were performed with the SANDER module of the AMBER9 program.[38,40] Equilibration protocols consisted of performing an initial optimization of the initial structures, followed by a slow heating up to the desired temperature. The heating was performed in 200 ps of constant volume MD, followed by 200 ps of MD at constant pressure. Once the system was equilibrated, the different production MD runs were performed. Frames were collected at 1 ps intervals, which were subsequently used to analyze the trajectories.

Free Energy Profiles for NO Escape. In order to study in detail the pH dependent NO migration mechanism in NP4, we determined the migration free energy profiles for NO escape in both low and high pH conformations. The free energy profiles were constructed by performing constant velocity multiple steered molecular dynamics (MSMD) simulations and using the Jarzynski's equality, which relates equilibrium free energy values with the irreversible work performed over the system which proceeds along a reaction coordinate from reactants to products.[41,42] In the present study, the reaction coordinate λ was chosen as the Fe−NO distance. Calculations were performed using a force constant of 200 kcal mol^{-1} Å^{-1} and pulling velocities of 0.01 Å/ps. The same simulation parameters for the MSMD simulations were already successfully used to study NO/O_2 migration in truncated hemoglobin N from *Mycobacterium tuberculosis*.[42,43] To compute each free energy profile, 20 different MSMD runs were performed in each case.

QM-MM Calculations. The initial structure for the QM-MM calculations were built starting from the crystal structures of NO bound NP4 (pH = 5.6) pdb code 1X8O, water bound NP4 (pH = 5.6) pdb code 1 × 8n, NO bound NP4 (pH = 7.4) pdb code 1 × 8q, and NH_3 bound NP4 (pH = 7.4) pdb code 1X8P.[24] In the NH_3 and water bound structures, the ligand was replaced by NO *in silico*. Each structure was protonated as mentioned above for each pH condition and optimized using classical MD. Starting from the four optimized structures, full hybrid QM-MM geometry optimizations of the NO bound and free proteins were performed using a conjugate gradient algorithm at the DFT level with the SIESTA code[44] using our own QM-MM implementation.[45] Only residues located less than 10 Å apart from the heme reactive center were allowed to move freely in the QM-MM runs. The SIESTA code showed an excellent performance for medium and large systems and also proved to be appropriate for biomolecules, and specifically for heme models.[46−49] For all atoms, basis sets of double plus polarization quality were employed. Previous works showed that QM-MM optimized structures and the binding energies are properly described with these basis set parameters. Calculations were performed using the generalized gradient approximation functional proposed by Perdew, Burke, and Ernzerhof.[50] The iron porphyrinate without the side chains and the relevant ligands, consisting of the proximal histidine and the NO ligand, were selected as the quantum subsystem. The rest of the protein unit, together with water molecules, was treated classically. The interface between the QM and MM portions of the

(32) Scott, E. E.; Gibson, Q. H.; Olson, J. S. *J. Biol. Chem.* **2001**, *276* (7), 5177−5188.
(33) Marti, M. A.; Crespo, A.; Capece, L.; Boechi, L.; Bikiel, D. E.; Scherlis, D. A.; Estrin, D. A. *J. Inorg. Biochem.* **2006**, *100* (4), 761−70.
(34) Menyhard, D. K.; Keseru, G. M. *FEBS Lett.* **2005**, *579* (24), 5392−5398.
(35) Berendsen, H. J. C.; Postma, J. P. M.; Van Gunsteren, W. F.; DiNola, A.; Haak, J. R. *J. Chem. Phys.* **1984**, *81*, 3684−3690.
(36) Van Gunsteren, W. F.; Berendsen, H. J. C. *Angew. Chem., Int. Ed. Engl.* **1990**, *29* (9), 992−1023.
(37) Ryckaert, J. P.; Ciccotti, G.; Berendsen, H. J. C. *J. Comput. Phys.* **1977**, *23*, 327−341.
(38) Hornak, V.; Abel, R.; Okur, A.; Strockbine, B.; Roitberg, A.; Simmerling, C. *Proteins* **2006**, *65* (3), 712−725.
(39) Bikiel, D. E.; Boechi, L.; Capece, L.; Crespo, A.; De Biase, P. M.; Di Lella, S.; Gonzalez Lebrero, M. C.; Marti, M. A.; Nadra, A. D.; Perissinotti, L. L.; Scherlis, D. A.; Estrin, D. A. *PCCP* **2006**, *8* (48), 5611−5628.
(40) Pearlman, D. A.; Case, D. A.; Caldwell, J. W.; Ross, W. S.; Cheatham Iii, T. E.; DeBolt, S.; Ferguson, D.; Seibel, G.; Kollman, P. *Comput. Phys. Commun.* **1995**, *91* (1−3), 1−41.
(41) Crespo, A.; Marti, M. A.; Estrin, D. A.; Roitberg, A. E. *J. Am. Chem. Soc.* **2005**, *127* (19), 6940−1.
(42) Xiong, H.; Crespo, A.; Marti, M.; Estrin, D.; Roitberg, A. E. *Theor. Chem. Acc.* **2006**, *116* (1−3), 338−346.
(43) Bidon-Chanal, A.; Marti, M. A.; Crespo, A.; Milani, M.; Orozco, M.; Bolognesi, M.; Luque, F. J.; Estrin, D. A. *Proteins* **2006**.
(44) Soler, J. M.; Artacho, E.; Gale, J. D.; García, A.; Junquera, J.; Ordejón, P.; Sánchez-Portal, D. *J. Phys.: Condens. Matter* **2002**, *14* (11), 2745−2779.
(45) Crespo, A.; Scherlis, D. A.; Marti, M. A.; Ordejón, P.; Roitberg, A. E.; Estrin, D. A. *J. Phys. Chem. B* **2003**, *107* (49), 13728−13736.
(46) Marti, M. A.; Capece, L.; Crespo, A.; Doctorovich, F.; Estrin, D. A. *J. Am. Chem. Soc.* **2005**, *127* (21), 7721−7728.
(47) Capece, L.; Marti, M. A.; Crespo, A.; Doctorovich, F.; Estrin, D. A. *J. Am. Chem. Soc.* **2006**, *128* (38), 12455−12461.
(48) Marti, M. A.; Scherlis, D. A.; Doctorovich, F. A.; Ordejon, P.; Estrin, D. A. *J. Biol. Inorg. Chem.* **2003**, *8* (6), 595−600.
(49) Crespo, A.; Marti, M. A.; Kalko, S. G.; Morreale, A.; Orozco, M.; Gelpi, J. L.; Luque, F. J.; Estrin, D. A. *J. Am. Chem. Soc.* **2005**, *127* (12), 4433−4444.
(50) Perdew, J. P.; Burke, K.; Ernzerhof, M. *Phys. Rev. Lett.* **1996**, *77* (18), 3865−3868.

system was treated by the scaled position link atom method,[51,52] adapted to our SIESTA code. Further technical details about the QM-MM implementation can be found elsewhere.[45] NO binding energies (ΔE_{NO}) were calculated as

$$\Delta E_{NO} = (E_{prot} + E_{NO}) - E_{prot-NO} \quad (1)$$

where $E_{Prot-NO}$ is the energy of the NO bound protein, E_{prot} is the energy of the free protein, and E_{NO} is the energy of the isolated NO molecule. ΔE_{NO} is the energy required to break the Fe−NO bond and NO protein interaction. The three energy terms required are obtained from the corresponding QM-MM calculations as described above. Total energies in QM-MM calculations may be decomposed into three contributions: E_{QM}, E_{QM-MM}, and E_{MM}, representing the energy associated with the quantum subsystem, the coupling between the quantum and the classical subsystems, and the classical system, respectively. In this case, $\Delta E_{NO(QM)}$ is the fraction of the binding energy that arises from the QM energies in the calculation. This energy represents mainly the contribution of the Fe−NO bond strength to the total energy in each protein. ΔE_{QM-MM} is the change in the QM-MM interaction energy with and without NO. It represents how much energy is gained (negative value) or lost (positive values) due mainly to NO bound interactions with the protein distal residues. The NO bound porphyrin was computed in the singlet spin state, and the free porphyrin, in the triplet spin state, which are the corresponding ground states.[39] It should be noted that although no entropy effects are included in our calculations, the entropy change associated with the ligand release reaction would contribute to lowering the ΔG compared to the ΔE_{NO} values calculated here. However, this contribution is expected to be similar in all considered cases, and thus, the results are still meaningful in a comparative view.

Results

The process of NO release from heme proteins is complex, and it is convenient to decompose in two processes to gain molecular insight. The first one corresponds to thermal breaking of the Fe−NO bond, a process governed by the interactions of the Fe−NO moiety within the protein. The second corresponds to the ligand migration process across the protein matrix from the active site and into the solvent. Experimentally the whole process can be characterized by the dissociation rate constant k_{off}. In our work, we have analyzed both processes separately using different techniques. To evaluate the strength of the Fe−NO bond and Fe−NO protein interactions we have computed ΔE_{NO} values using a QM/MM scheme. The second process, which corresponds to ligand migration from the active site and into the solvent, has been evaluated in our work by using Multiple Steered MD and Jarzynski's inequality in order to obtain the whole free energy profile.

QM-MM Calculations. In order to study the effect of the protein conformation and heme structure on the Fe−NO bond, we performed QM-MM calculations using as initial structures the four high-resolution crystal structures, obtained at pH = 5.6 with NO, pH = 5.6 with coordinated water, pH = 7 with NO, and pH = 7.4 with NH_3 bound, respectively. This set of structures displays an increasing opening of the AB and GH loops. For all cases, we performed geometry optimizations for the corresponding Fe^{III}−NO complexes and the free proteins. In order to separately analyze the influence of the protein contribution and the heme conformation, we also present the differences in QM binding energy $\Delta E_{NO(QM)}$ and in ΔE_{QM-MM} contributions to the total binding energy. The results are shown in Table 1.

Table 1. Selected NP−NO Complexes Geometrical and Energetic Parameters[a]

protein	pH5.6-NO	pH5.6-wat	pH7.4-NO	pH7.4-NH_3	isolated-heme
Fe−N	1.66	1.65	1.65	1.66	1.65
NO	1.17	1.17	1.16	1.16	1.17
Fe−N−O	169.5	174.0	177.9	178.5	178.3
ΔE_{NO}	39.9	39.2	40.7	43.24	36.6
$\Delta E_{NO(QM)}$	36.4	36.3	37.8	38.74	-
ΔE_{QM-MM}	−3.7	−3.5	−4.8	−5.2	-

[a] Geometrical and energetic parameters for the NP4-NO optimized structures. Data correspond to four high-resolution crystal structures mentioned before and an isolated porphyrin. Distances are shown in angstroms; angles, in degrees; and energies, in kcal/mol. ΔE_{NO} given by eq 1 is the energy required to break the Fe−NO bond and NO protein interaction obtained from the QM-MM calculation. $\Delta E_{NO(QM)}$ is the fraction of the binding energy that arises from the QM energies. ΔE_{QM-MM} is the contribution to the coupling QM-MM terms to the binding energy. For a detailed explanation of these terms see the Materials and Methods section.

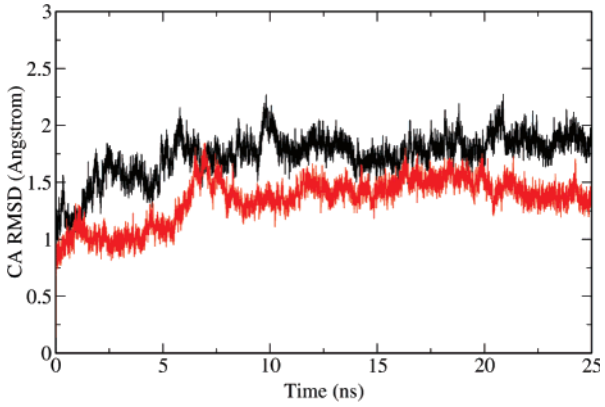

Figure 1. Cα rmsd (angstrom) for NO bound runs. The black line shows the rmsd against the pH 7.4 $-NH_3$ structure along the high pH NP4-NO MD run. The red line shows the rmsd against the pH 5.6 −NO structure along the low pH Np4-NO MD run.

The results show that the NO binding is similar in all cases being slightly larger in the pH 7.4 $-NH_3$ structure. The comparison of the Fe−NO structure shows that, in both open conformations, NO may assume a linear conformation which is the minimum energy configuration for the isolated heme, whereas, in the closed conformation, it is slightly bent. The ΔE_{QM-MM} results show that in all cases the protein interacts favorably with the bound NO molecule (all values are negative) but the interaction is more favorable in the high pH conformation. These results indicate that the closed conformation does not leave enough space to accommodate the NO properly. However, the differences are small and are not expected to produce a significant difference in the NO dissociation rate.

MD Simulations of the NO Protein Complexes. We started the analysis of the NO bound MD simulations for the NP4 structures at both pH conditions from now on termed low pH and high pH simulations. The stability of the structures, with the corresponding assigned protonation states, was checked along the 25 ns MD simulation for each case. Figure 1 shows the root-mean-square deviation Cα-rmsd along each simulation with respect to the corresponding reference X-ray structures.

As can be seen in Figure 1, both structures remain stable, with the simulation corresponding to pH 7.4 presenting a slightly

(51) Eichinger, M.; Tavan, P.; Hutter, J.; Parrinello, M. *J. Chem. Phys.* **1999**, *110* (21), 10452−10467.
(52) Rovira, C.; Schulze, B.; Eichinger, M.; Evanseck, J. D.; Parrinello, M. *Biophys. J.* **2001**, *81* (1), 435−445.

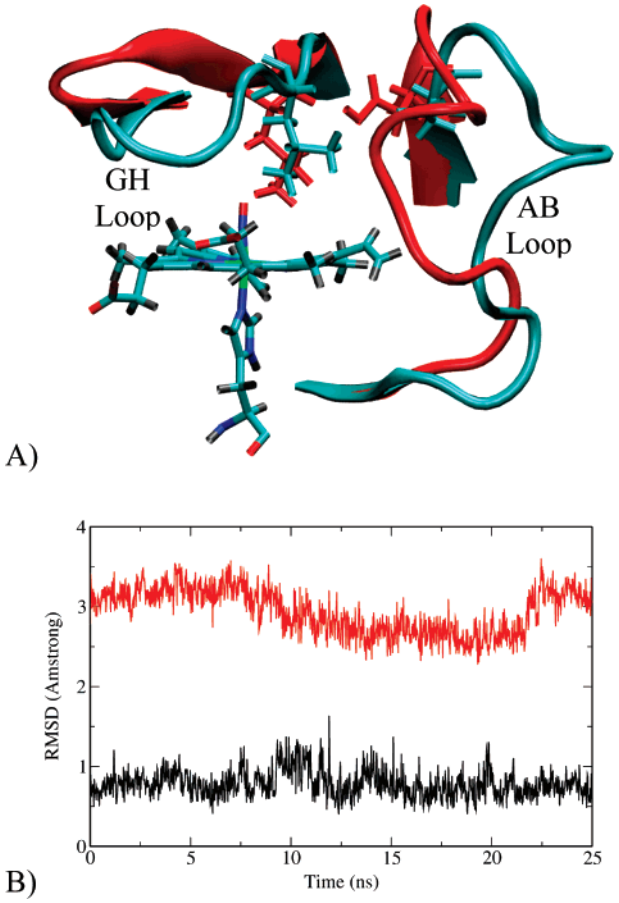

Figure 2. (A) Mean structures AB and CG loops conformation at pH = 7.4 and 5.6, depicted in cyan and red, respectively. (B) AB and CG loops (residues 28 to 40 and 124 to 132) Cα-rmsd along the low pH NP4-NO MD run using as references the low and high pH average structures, depicted in black and red lines, respectively.

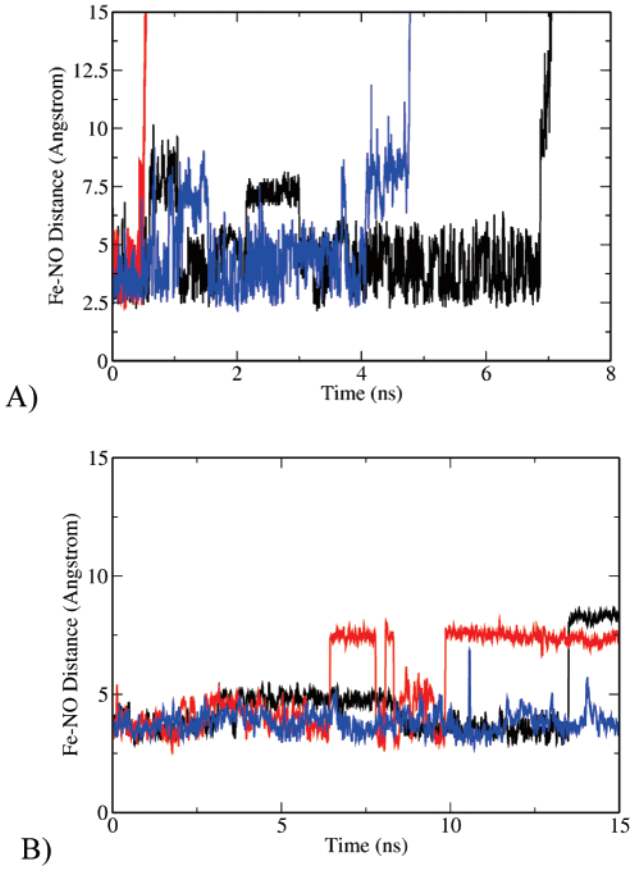

Figure 3. Fe−NO distance as a function of time for the NO free MD simulations (A) NP4:NO high pH and (B) NP4:NO low pH.

higher deviation with respect to the crystal structure. As already mentioned, the pH dependent conformational change in NP4 is mainly centered in the AB and GH loops. Figure 2 shows the heme group and both loop regions for the mean structures obtained for each low and high pH 25 ns MD run. The figure also indicates that the interaction of protonated Asp30 and the carbonyl of Leu130 in the low pH structure is maintained along the time scale of our simulation. This interaction is lost at higher pH due to the ionization of Asp30 and is supposed to be one of the key determinants of the conformational change. In the high pH conformation the carbonyl of Leu 130 interacts instead with the NH_3 from Alanine 1 (see Figures 1 and 2 in Supporting Information). Visual inspection of the MD run and of the mean structures shows that the different loop conformations are maintained in each simulation, corroborating that the assignation of differential protonation state of Asp30 is the key issue to determine the conformational difference between low and high pH conformations.

To further corroborate the stability of each conformation we computed the AB and GH loop residue Cα-rmsd in both simulations against each average structure. The results for the low pH conformation run are shown in Figure 2B. As expected, along the dynamics the loop structure remains similar to the low pH reference but shows differences compared to the high pH conformation. Similar results are observed by computing the Cα-rmsd of the high pH MD run against both reference structures (see Figure 5 in Supporting Information). The analysis of the overall results of the NO bound protein simulations indicate that the structures are stable and that starting from the corresponding structures with differential assignation of Asp30 protonation state is enough to ensure that AB and GH loops retain the experimentally observed conformations.

NO Free MD Runs. To characterize the ligand escape process in both conformations we performed several additional MD simulations (three for each pH condition) starting from an equilibrated NO-bound structure but without constraining the NO to be bound to the iron. In this case, the ligand is free to move inside the protein. We have only explored the range of Fe−NO distances relevant to the NO escape process. At distances larger than 3 Å bonding interactions are supposed to be inoperative. We checked the stability of these simulations as mentioned above, and again both structures remained stable, with low rmsd values using the corresponding X-ray structures as reference. Figure 3 shows the Fe−NO distance versus time for the corresponding MD simulations for each of the two pH conditions.

Figure 3 shows a completely different picture for both conditions. In the first place, in the high pH condition NO can move much more freely, with NO distances continuously varying between 3 and 8 Å, corresponding to NO moving in the distal pocket (DP) of NP4. The most striking fact is that in all three independent runs after NO moves away from the iron it escapes from the protein and goes into the bulk solvent. As will be shown later, the exit path followed by the NO is toward the AB loop. At lower pH the picture is quite different, and

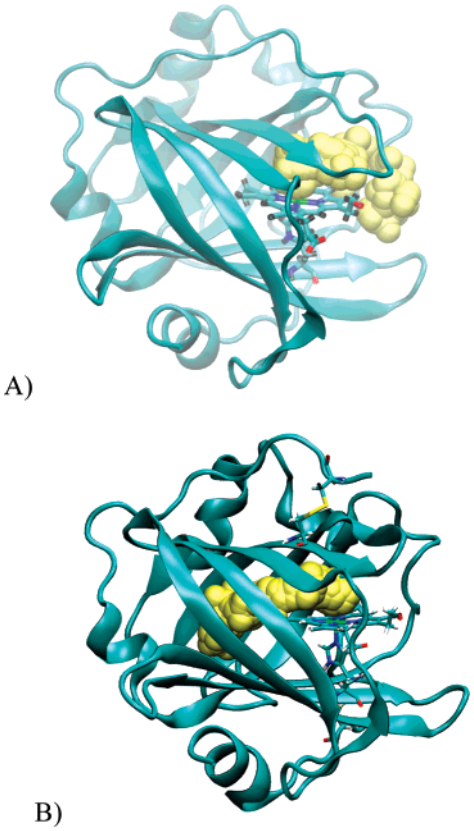

Figure 4. NO location in NP4 along a selected SMD run. (A) High pH situation. (B) Low pH condition. NO positions are shown as yellow spheres, protein is shown as blue ribbons, and the heme group and proximal histidine are shown as sticks.

NO is much more restricted in the active site. We did not observe any NO escape event during the time scale of our simulation.

Free Energy Profiles of NO Escape. To better characterize the NO escape mechanism and to obtain a reliable estimation of the NO escape probability at both pH conditions, we performed 20 MSMD simulations, pulling the NO out of NP4 for each protein conformation. The chosen reaction coordinate was the Fe−NO distance, without any angular restraints. This allows NO to explore any possible way out of the protein. All MSMD simulations were started from a snapshot of NO located in the DP, either from the above-mentioned NO free simulation or from MD simulations in which NO was constrained to remain in the DP, to avoid escape at high pH conditions. The starting snapshots were separated in 1 ns intervals. As expected from the previous NO free run in 21 out of 22 MSMD runs at the high pH condition, the NO escapes NP4 through the exit path that goes along the AB loop. As an example, Figure 4 shows the position of the NO molecule along one selected SMD run. The corresponding works present a barrier distribution ranging from 2 kcal/mol up to 10 kcal/mol (shown in the Supporting Information) yielding a free energy profile with a barrier of ∼3 kcal/mol, as shown in Figure 5.

As expected, the results obtained from the SMD runs at low pH conditions are completely different. The analysis of the work vs RC profiles (shown in the Supporting Information) suggest that the barrier is too high for NO to escape. The first evidence comes from following the NO trajectory in the 20 SMD runs. Visual inspection of these runs shows that, in 11 of these runs,

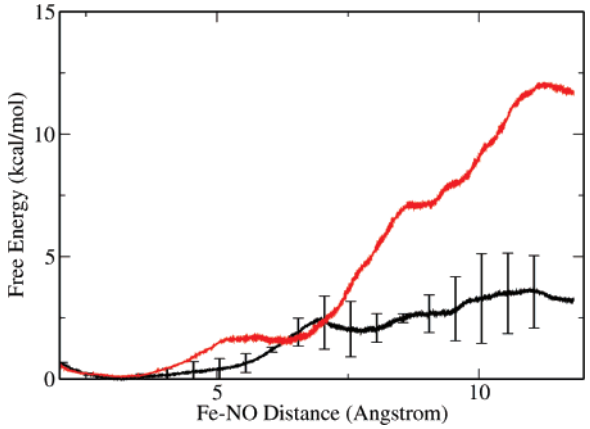

Figure 5. Free energy profiles for NO escape from NP4. Results for the high pH and low pH structures are depicted using black and red lines, respectively. In the high pH profile the data correspond to mean ±SD of two independent sets of 10 MSMD calculations.

NO does not escape but instead migrates deep into the protein matrix. Figure 4B shows the position of the NO molecule along one selected SMD run in which this is the case. In the 9 remaining SMD runs NO actually manages to escape by overcoming quite high barriers. Moreover, in only two runs NO escapes to a path that is similar to the one followed by the NO in the high pH conformation. Using these 9 SMD runs in the low pH condition where NO escapes, an estimation of the free energy for ligand escape can be obtained and compared with that obtained at high pH, as shown in Figure 5.

The results shown in Figure 5 confirm that NO easily escapes from NP4 when it is in the high pH conformation and that the protein closes and blocks the way in low pH conditions. In the low pH conformation the barrier for NO escape is too high, and when the NO is pulled away from the iron it prefers to move deeper inside the protein matrix.

Discussion

NO Escape Path. Combining the information from the NO free MD and the MSMD simulations at high pH the path followed by the NO along the exit pathway can be analyzed in atomic detail (Figure 6). Once the Fe−NO bond is broken, NO remains in the distal pocket (DP) (at around 3.5 Å from the heme iron) surrounded by the side chains of hydrophobic residues Leu 123, Leu 133, Leu130, and the CH_3 of Thr121 (Figure 6). Interestingly, and in agreement with the observed experimental data, along the MD simulation one or two water molecules are also observed near this zone. From the DP NO can move upward away from the heme but no further than 6 Å, since this way is blocked by the backbone of residues 121 to 123 and 131 to 133 (Figure 6). Along the way out the NO instead passes next to Leu 133 toward the C and D indolic ring side of the heme, where it remains surrounded by the side chains of residues Val36 and Pro37. Several water molecules are present in this site, and it is well connected with the bulk solvent. The small barrier of ∼2.5 kcal/mol observed in the profile at ∼7 Å is related mainly to surpassing Leu133, while the observed small free energy increase at ∼10 Å is due to the NO entering the solvent.[32]

The same analysis can be performed for the low pH runs. In this case, after the Fe−NO bond is broken the ligand remains in the DP surrounded by the same residues as in the high pH

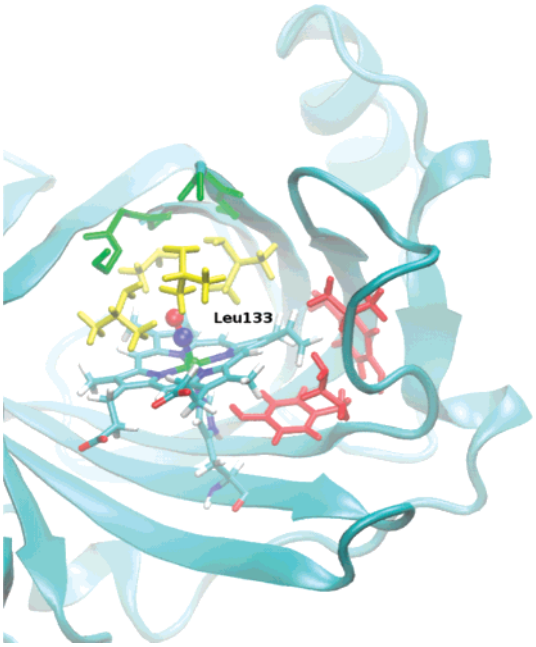

Figure 6. Residues involved in the NO exit path in the high pH simulations. NP4 is shown as ribbons, and relevant residues are shown as sticks. Leu 123, Leu133, and Leu 130 are shown in yellow; the backbones of residues 121 to 123 and 131 to 133 are shown in green; and Val36, Pro37, and Tyr28 are shown in red.

condition case. However, due to differential loop conformation (Figure 2) Leu 133 does not allow NO to pass. Moreover, at low pH Val36 and Pro37 (shown in red in Figure 6) are in close contact with the heme group's C and D rings, also contributing to blocking the escape path (Figure 7B). Notably, the Asp30-Leu130 interaction also blocks possible NO escape from above. Therefore, instead of moving toward the solvent, in the low pH MSMD runs NO moves further inside the protein (as shown in Figure 6) passing next to Leu123 and toward Tyr105.

Our results are able to explain with atomic detail how the different conformations observed at low and high pH conditions differentially modulate NO release. When going from a low pH to high pH condition, Asp30 becomes deprotonated and its interaction with Leu130 is destroyed. This allows the AB and GH loops to change conformation (see Figure 2) opening a way out from the protein active site and into the solvent. Interestingly, in the high pH conformation, the interaction between Asp129 and protonated Asp35 is also lost. Figure 7 shows the distance between the C atoms of both carboxylic groups in both simulations. In the low pH simulation, both carboxylate moieties interact during the time scale of the simulation, but at high pH Asp35 is pointing away from Asp129 and into the solvent. Although previous studies showed that Asp35 is likely to be protonated at both pH conditions our results show that, at higher pH values, Asp35 is more likely to move into the solvent and become charged.

The conformational change in the AB and GH loops mainly moves the AB loop away from the heme disrupting the interaction between Val36, Pro37 (depicted in red in Figure 6) and the CD side of the heme (Figure 7B). As a consequence, Val36 and Leu133 are more separated and mobile (Figure 7C) allowing NO to easily pass next to Leu133 and through the space left due to the movement of Val36 and Pro37.

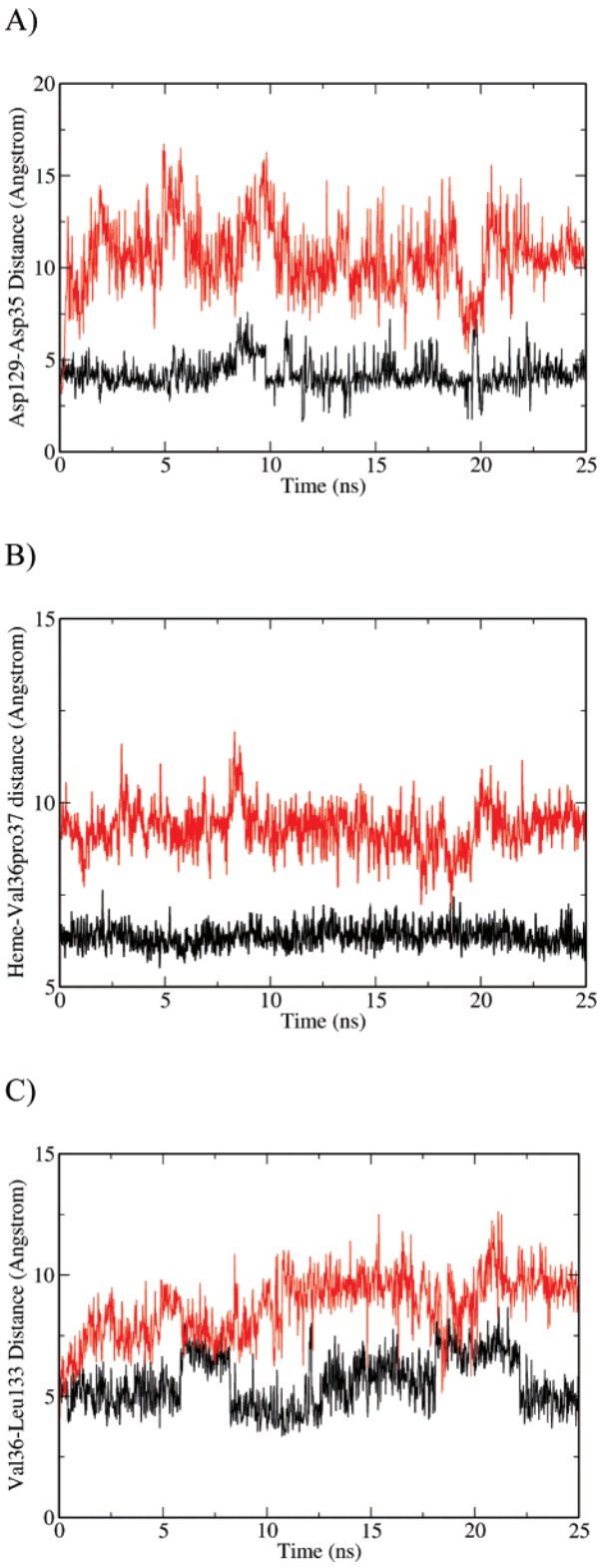

Figure 7. (A) Asp129-Asp35 carboxylic C atoms distance as a function of time. (B) Heme CD side Val36 side chain distance as a function of time. (C) Val36-Leu133 sidechain distance as a function of time. Results obtained at the low and high pH structures are depicted with black and red lines, respectively.

Conclusion

Our results show that the pH modulation of the NO rate escape from NP4 arises not from a weaker NO interaction in the high pH conformation but from faster migration of the NO

through the protein. The QM/MM results show that the Fe−NO bond strength is almost independent of the NP4 conformation and that bound NO interactions with the residues located in the distal cavity are similar in all four pH dependent structures. Moreover, these interactions were slightly favorable in the high pH condition, an unexpected result considering that in this condition NO is released. All of our MD results show unequivocally that NO can only escape the NP4 distal pocket in the high pH conformation. In the low pH conformation NO does not escape but rather migrates further inside the protein and probably rebinds to the heme easily. Our results are consistent with experimental data which suggested that breaking of the Fe−NO bond interaction was not responsible for the pH dependent NO release.[17] Our results are also consistent with FTIR studies of CO and NO migration which show that the pH dependent NO release is achieved due to differential migration rates in both the low pH (closed) and high pH (open) conformations.[53] Furthermore, and consistent with our data, no secondary docking sites were observed along the NO escape path except for a Xenon site detected in the proximal side of the heme.[53] Interestingly, in the low pH NO free and MSMD runs, the NO molecule is found in this site during a significant time of the simulation.

Concerning the mechanism proposed by Montfort's group (Scheme 1), our data suggest that pH independent k_1 and k_{-1} could be associated to thermal breaking of the Fe−NO bond and that pH dependent k_2 and k_{off} correspond to ligand migration and/or loop reorganization. The nature of the different rates observed fro NP4′-NO and NP4″-NO can, in this scenario, be attributed to different protein conformations presenting slightly different rates. As mentioned above, the MSMD work profiles present NO escape barriers that differ by several kcal/mol and could therefore correspond to these different conformations.

Our results also confirm that differential protonation of Asp30 is probably the main process responsible for the conformational change. Our results also point to a key role played by Asp35 as differentially stabilizing both conformations.

Another interesting point arising from our results can be summarized in the question of why a heme protein is required for transporting NO if binding of NO to the iron plays no role in the transport mechanism. In this line of thought, our results show that NO binding to the iron allows the high reactive NO molecule to be safely carried when bound to the iron. However, the chemical nature of Fe−NO bond in isolated heme model systems indicates that the bond is very strong when the iron is reduced and weak when it is oxidized. Therefore, in this scenario, the conformational change in the protein allows the pH-dependent regulation by controlling NO diffusion. The relatively weak Fe(III)−NO bonds allow easy thermal breakage, but in the low pH condition NO remains trapped and rebinds. Once the bond is broken in the high pH condition, NO has an open way out of the protein.

It is relevant to note that, to our knowledge, this is the first case where the mechanism of a heme protein ligand affinity regulation directly linked to a conformational change has been explained at molecular detail using computer simulations. Understanding conformational regulation of ligand affinity is of primary interest since it may play a crucial role in regulating heme protein function.

In summary, we have shown that NO escape from NP4 is determined by differential NO migration rates and not by a difference in the Fe−NO bond strength at different pH values. Although most proteins control ligand affinity by modulating the bond strength to the iron, NP4 has evolved a cage mechanism that traps the NO at low pH and releases it upon cage opening when the pH rises.

Acknowledgment. This work was supported by grants from the ANPCYT (National Science Agency of Argentina), CONICET, and University of Buenos Aires to D.A.E. M.A.M. thanks CONICET for a Doctoral fellowship. Computer resources were provided by the Large Allocations Resource Committee through Grant TGMCA05S010 to A.E.R.

Supporting Information Available: Distance vs time plot between Asp30 and Leu130 (Figure S1), Distance vs time plot between Leu130 and Ala1 (Figure S2), Work vs RC Profiles for MSMD runs, at the high pH and low pH condition. This material is available free of charge via the Internet at http://pubs.acs.org.

JA075565A

(53) Nienhaus, K.; Maes, E. M.; Weichsel, A.; Montfort, W. R.; Nienhaus, G. U. *J. Biol. Chem.* **2004**, *279* (38), 39401−39407.